

Colloidal Gold Nanoclusters Spiked Silica Fillers in Mixed Matrix Coatings: Simultaneous Detection and Inhibition of Healthcare-Associated Infections

Shahad K. Alsaieri, Mohammed A. Hammami, Jonas G. Croissant, Haneen W. Omar, Pradeep Neelakanda, Tahir Yapici, Klaus-Viktor Peinemann, and Niveen M. Khashab*

Healthcare-associated infections (HAIs) are the infections that patients get while receiving medical treatment in a medical facility with bacterial HAIs being the most common. Silver and gold nanoparticles (NPs) have been successfully employed as antibacterial motifs; however, NPs leaching in addition to poor dispersion and overall reproducibility are major hurdles to further product development. In this study, the authors design and fabricate a smart antibacterial mixed-matrix membrane coating comprising colloidal lysozyme-templated gold nanoclusters as nanofillers in poly(ethylene oxide)/poly(butylene terephthalate) amphiphilic polymer matrix. Mesoporous silica nanoparticles–lysozyme functionalized gold nanoclusters disperse homogeneously within the polymer matrix with no phase separation and zero NPs leaching. This mixed-matrix coating can successfully sense and inhibit bacterial contamination via a controlled release mechanism that is only triggered by bacteria. The system is coated on a common radiographic dental imaging device (photostimulable phosphor plate) that is prone to oral bacteria contamination. Variation and eventual disappearance of the red fluorescence surface under UV light signals bacterial infection. Kanamycin, an antimicrobial agent, is controllably released to instantly inhibit bacterial growth. Interestingly, the quality of the images obtained with these coated surfaces is the same as uncoated surfaces and thus the safe application of such smart coatings can be expanded to include other medical devices without compromising their utility.

1. Introduction

A key challenge in controlling the spread of healthcare-associated infections (HAIs) is the ability of microbes to survive, grow, and colonize on hospital surfaces and patient care devices. In the past 20 years these infections have increased by 36%, escalating the urgency for developing antibacterial surfaces to prevent bacterial growth and, hence, biofilm formation.^[1] Antimicrobial coating materials have thus been designed to protect surfaces prone to bacterial contamination. One of the most used antimicrobial ingredients in clinical technologies are nanoscaled silver (Ag) particles due to their ability to slowly release antimicrobial silver ions.^[2–5] For example, Ag nanoparticles (NPs)-doped polyethyleneimine constituted an effective antibacterial surface coating material.^[6–9] Nonetheless, the extensive exposure of bacteria to Ag-containing membranes endowed the development of Ag-resistant microorganisms.^[10–12] Recent reports also revealed that the leaching of Ag NPs from packaging and storage products remains a major health concern.^[13] Other biocidal agents were incorporated into coating matrices to enhance their antibac-

terial properties, such as zinc oxide particles,^[14] triclosan,^[15–17] eugenol,^[18,19] and antibiotics,^[20] but again leaching continued to be a major drawback. These studies were mainly focused on the optimization of the antibacterial activity of the coating matrices with no bacterial sensing capabilities.^[21–24]

The simultaneous sensing and inhibition of bacteria; contamination has been investigated in other studies.^[25–28] Dam and co-workers specifically targeted and detected infections caused by Gram-positive bacteria using fluorescently labeled vancomycin.^[26,29] Jenkins and co-workers described a thin film functionalized with vesicles to detect and inhibit the bacterial growth by a selective release of antimicrobial agents only in the presence of pathogenic bacteria.^[30] Lysozyme functionalized gold nanoclusters (AuNCs) were used to detect bacteria through the multivalent interactions between lysozyme and N-acetylglucosamine on the peptidoglycans on bacterial cell walls.^[31–33] Nonetheless, the development of a biocompatible

S. K. Alsaieri, M. A. Hammami, Dr. J. G. Croissant,
H. W. Omar, Prof. N. M. Khashab
Smart Hybrid Materials Laboratory (SHMs)
Advanced Membranes and Porous Materials Center
King Abdullah University of Science and Technology
(KAUST)
Thuwal 23955-6900, Saudi Arabia
E-mail: Niveen.khashab@kaust.edu.sa

Dr. P. Neelakanda, Prof. K.-V. Peinemann
Advanced Membranes and Porous Materials Center
King Abdullah University of Science and Technology (KAUST)
Thuwal 23955-6900, Saudi Arabia

Dr. T. Yapici
Analytical Core Lab
King Abdullah University of Science and Technology (KAUST)
Thuwal 23955-6900, Saudi Arabia

DOI: 10.1002/adhm.201601135

coating material for medical devices which could simultaneously detect and inhibit bacterial growth without leaching of the antimicrobial agent remains challenging to this day.

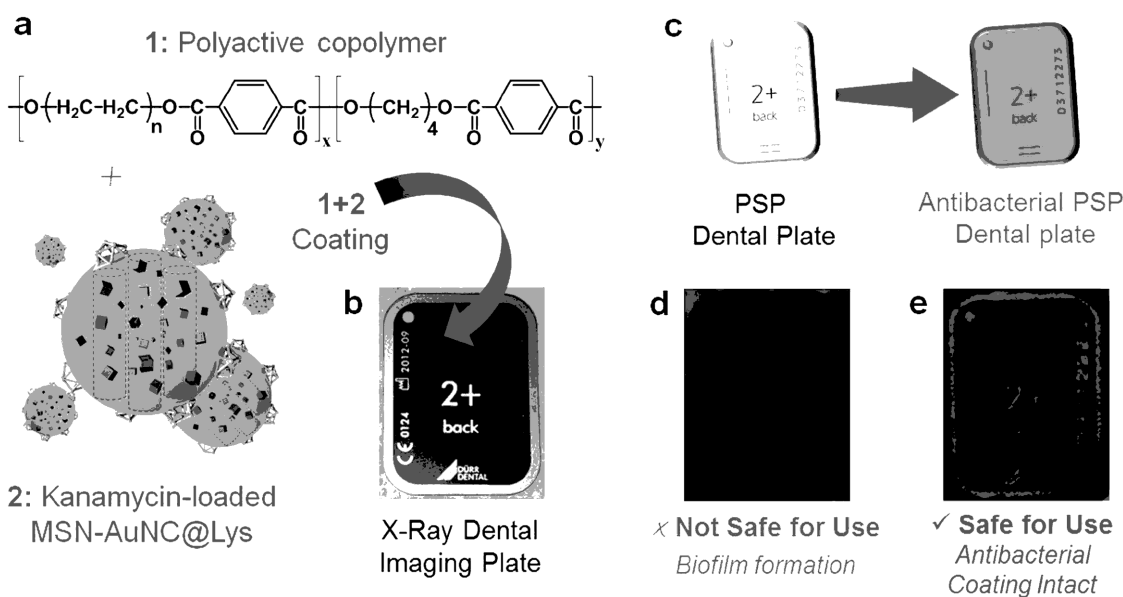
Herein, we report the fabrication of a smart antibacterial polymer coating containing gold nanoclusters-lysozyme (AuNC@Lys) colloids capping kanamycin (Kana)-loaded mesoporous silica nanoparticles (MSN) as antimicrobial nanofiller, applied on a medical device for safer X-ray dental imaging. The electrostatic self-assembly of negatively charged and fluorescent AuNCs onto positively charged aminated MSN provided bacteria-responsive nanofillers into the coating for the detection and inhibition of bacterial contamination. Upon encountering bacteria, AuNC@Lys detached from the MSN surface due to the interaction of lysozyme with the bacterial cell wall, and the release of entrapped Kana antibacterial cargos occurred. Concurrently, the loss of the red fluorescence of AuNC@Lys was efficiently detected affording a qualitative bacterial sensing platform. The MSN–AuNC@Lys nanofiller was then uniformly dispersed into poly(ethylene oxide)/poly(butylene terephthalate) (PEO–PBT, of commercial name polyactive) coating material without particle leaching (Scheme 1). This biocompatible mixed-matrix membrane was successfully scaled-up with high uniformity and reproducibility. The novelty of the work could be summarized as follows: (1) design and application of a novel bacteria-responsive gold nanoclusters@lysozyme-mesoporous silica nanocontainer for bacteria sensing and controlled-release of antibacterial agents; (2) design and application of a bacteria-responsive smart mixed polymer membrane; (3) a real-life application of the system via the spin coating of the smart membrane on dental imaging plates, which are reusable dental care products suffering from high risk of oral bacteria contamination. This smart coating successfully detected and inhibited bacterial infection while maintaining the quality of the dental images obtained with these plates.

2. Results and Discussion

2.1. Fabrication and Characterization of the MSN–AuNC@Lys Nanofillers

The gold nanoconjugates were first synthesized according to a previously published procedure^[34] and applied for their well-known red-NIR photostable emission and high quantum yield.^[35,36] The synthesis of AuNC@Lys involved the reduction of Au(III) ions in the presence of lysozyme at 37 °C upon the addition of sodium hydroxide. The AuNC@Lys nanoconjugates were characterized by transmission electron microscopy (TEM) which displayed ≈2 nm nano-objects (Figure S1a, Supporting Information), and fluorescence spectroscopy showed the typical broad red emission of the clusters centered at 680 nm (Figure S1b, Supporting Information). The charged of AuNC@Lys was negative (–7 mV) in neutral conditions according to Zeta potential analyses (Figure S1c, Supporting Information).

The MSN–AuNC@Lys nanofillers were then prepared, starting with the sol–gel synthesis of mesoporous silica nanocontainers^[37] which have attracted tremendous attraction for their biocompatibility^[38–40] and controllable structure.^[41–44] In order to electrostatically bind the negatively charged AuNC@Lys to MSN, the surface functionalization of the nanocontainers was carried out with aminopropyltriethoxysilane affording MSN–NH₂ (+24 mV). Fast Fourier transform infrared (FTIR) spectroscopy confirmed the preparation of aminated silica particles with the ν_{Si–O} and ν_{N–H} stretching vibration modes at 1089 and 1385 cm^{–1}, respectively (Figure S2, Supporting Information). In order to meet the requirements of a drug release carrier nanofiller (Figure 1), the designed particles had to be non-aggregated and porous. The porosity was confirmed by the type IV N₂-adsorption–desorption isotherm typical of mesoporous materials, the high Brunauer–Emmett–Teller



Scheme 1. Fabrication of the a) polyactive copolymer doped with Kana-loaded MSN–AuNC@Lys nanofiller b) for the coating of an X-ray dental plate device. The coating material provides c,d) antimicrobial and d,e) contamination detection features to the device. The contamination can be assessed by the naked eye simply by the color change of the dental plate exposed to UV light, providing a practical medical device.

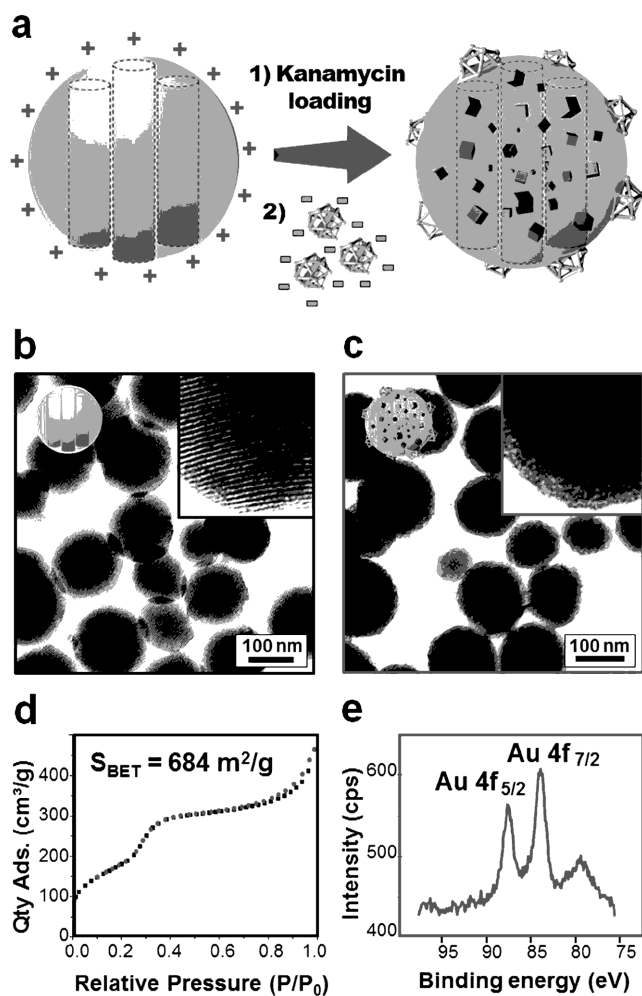


Figure 1. a) Representation of the preparation of Kana-loaded MSN-AuNC@Lys; TEM micrographs of MSN-NH₂ b) before and c) after coating of AuNC@Lys. d) Nitrogen sorption isotherm of MSN-NH₂ NPs. (e) XPS of Kana-loaded MSN-AuNC@Lys in the 4f gold region.

surface area of 684 m² g⁻¹, and the pore size distribution of MSN-NH₂ centered at 2.3 nm according to the Barret-Joyner-Halenda theory (Figure 1e). The absence of aggregation was shown by TEM which displayed well-dispersed MSN-NH₂ 150 nm large carriers with a long-range mesoporous order (Figure 1b).

The preparation of MSN-NH₂ containers capped with AuNC@Lys was then investigated. Note that both AuNPs and AuNCs have been reported as pore capping agents due to their strong electrostatic interactions with protonated amino groups as well as their high biocompatibility.^[45–47] The preparation of MSN-AuNC@Lys was clearly confirmed visually via TEM which showed a rough particle surface typical of protein-coated MSN (Figure 1c).^[45] This successful capping was further supported by FTIR which depicted the appearance of several vibration modes of AuNC@Lys on the spectrum of MSN-AuNC@Lys, such as the $\nu_{C=O}$ (1674 cm⁻¹), $\delta_{N-H \text{ arom}}$ (1545 cm⁻¹), and δ_{N-H} (1230–1380 cm⁻¹) of lysozymes (Figure S2, Supporting Information). The presence of gold atoms was also directly confirmed by high-resolution X-ray photoelectron spectroscopy

(XPS) with the presence of the Au 4f_{5/2} and 4f_{7/2} peaks respectively centered at 83.9 and 87.6 eV which is associated with Au⁰ and Au¹⁺ typical of gold nanoclusters (Figure 1d).^[48]

The loading of the pores of MSN-NH₂ with Kana bacteriocidal agents followed by their capping with AuNC@Lys nanoconjugates was then performed (Figure 1a). The size distribution of the pores (\approx 2 nm) of the particles was well-suited for the loading of the drugs (\approx 1 nm), and the subsequent pore capping with AuNC@Lys (\approx 2 nm). The Kana loading inside NH₂-MSN was carried out in phosphate buffer saline (PBS) at room temperature for 24 h followed by the addition of AuNC@Lys. The amount of loaded Kana was detected by UV-vis and it was found to be 350 mg g⁻¹. It was calculated via analyses of drug supernatants. The rhodamine B (RhB) violet dye was also used as a control cargo to verify the proper operation of the system by monitoring the fluorescence. Photographs of cargo-free and cargo-loaded particle suspensions before and after centrifugation supported the stable loading of the cargos in the particles (Figure S3, Supporting Information).

2.2. Sensing and Antibacterial Properties of MSN-AuNC@Lys Nanofillers

The sensing and antibacterial properties MSN-AuNC@Lys associated with the controlled release application of the system were then tested in the presence *Escherichia coli* (*E. coli*) bacteria (Figure 2a). *E. coli* was selected as a model bacterium to study the antibacterial activity of Kana-loaded MSN-AuNC@Lys as it is a well-characterized and a medically relevant bacterium. *Bacillus safensis* was used as a model bacterium for Gram-positive bacteria. All antibacterial activity tests were performed in triplicates and were carried out at different times to ensure the experimental reproducibility. The mechanism of the drug release system involved the adsorption of the particles in the bacteria upon bacterial contamination, followed by the degradation of the bacterial cell wall by lysozyme which would in turn quench the gold fluorescence (Figure 2a). Experimental observations showed that the fluorescence of AuNCs did gradually quench over time (Figure 2b), which revealed that the fluorescence depended on the lysozyme catalytic activity. Beginning with the model dye cargo, RhB-loaded MSN-AuNC@Lys were then incubated with *E. coli* (1.6×10^8 CFU mL⁻¹) at 37 °C under gentle shaking to assess the bacteria-responsiveness of the particle. The particles depicted a controlled release of RhB in bacteria growing media Luria broth (LB) and no release was detected in the absence of *E. coli* (Figure 2c). Similar conclusions were observed for Kana-loaded particles (Figure 2d). Interestingly, the release of both cargos was delayed for about 20 min. This was consistent a study Li and Wang, which suggested that nanomaterial-bacteria interactions are initiated in 10 min and that the cell wall destruction occurs in 30 min.^[33]

2.3. Biocompatibility of MSN-AuNC@Lys Nanofillers

The biocompatibility of AuNC@Lys-capped Kana-MSN nanofillers was then tested in two different cell lines MCF-7 and HCT-116. Their cytotoxicity was assessed by the

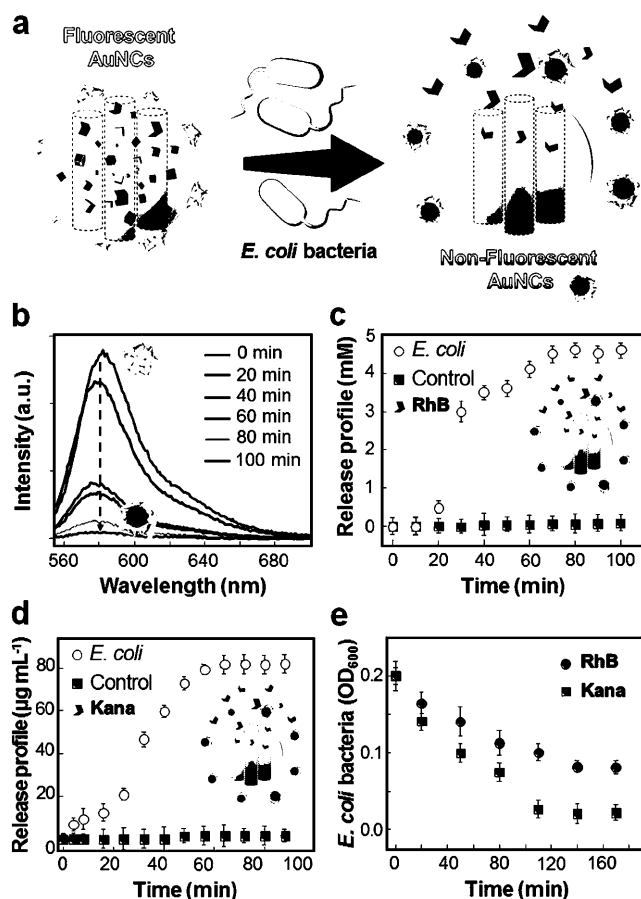


Figure 2. a) Schematic illustration of the bacteria-triggered cargo release from MSN–AuNC@Lys NPs. b) Fluorescence emission spectra of AuNC@Lys: as the activity of lysozyme increases, the fluorescence of AuNCs decreases. Release profiles of c) RhB-loaded and d) Kana-loaded MSN–AuNC@Lys in the presence of *E. coli* bacteria or in LB. e) Kinetics of the antibacterial activity of MSN–AuNC@Lys loaded with RhB and Kana (20 g mL^{-1}) in LB broth at initially fixed bacteria concentration.

3-(4,5-dimethylthiazol-2-yl)-2,5 diphenyltetrazolium bromide (MTT) assay and the results were compared with the controls. The data obtained proved that the MSN–AuNC@Lys nanofillers were biocompatible even at the high concentration of $200 \text{ }\mu\text{g mL}^{-1}$ in the two different cell lines (Figure S4, Supporting Information).

2.4. MSN–AuNC@Lys Bacterial Inhibition Kinetics

The *E. coli* inhibition kinetics in response to its interaction with cargo-loaded MSN–AuNC@Lys at the concentration of $20 \text{ }\mu\text{g mL}^{-1}$ were studied over 3 h (Figure 2e). The antibacterial activity was related to the activity of AuNC@Lys. Compared to the control point ($\text{OD}_{600}: 0.2 = 1.6 \times 10^8 \text{ CFU mL}^{-1}$), the *E. coli* viability decreased by 50% in 170 min when the RhB inactive cargos was used due to the activity of AuNC@Lys (as discussed later with Figure 3c). Note that, the activity of MSN–AuNC@Lys was similar to the one of RhB-loaded MSN–AuNC@Lys (data not shown). Incorporating the antibacterial Kana drugs into

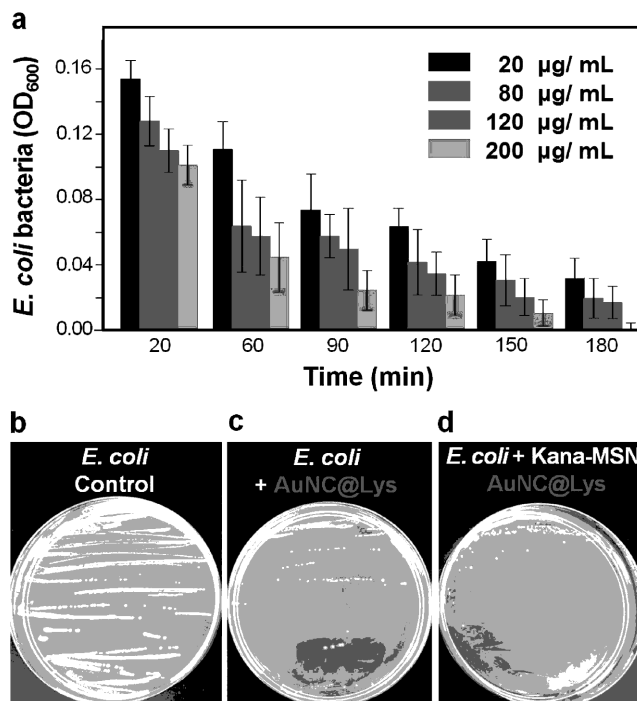


Figure 3. a) Antibacterial activity of different concentrations of NPs over time toward *E. coli* ($1.6 \times 10^7 \text{ CFU mL}^{-1}$). b–d) Photographs of Petri dishes showing the d) antimicrobial activity of Kana MSN–AuNC@Lys against *E. coli* compared with b) an *E. coli* control and c) the activity of AuNC@Lys. A portion of the LB broth bacterial suspension was streaked on LB agar. A system free of *E. coli* was used as a control to compare the bacterial growth.

the pores of the nanofillers, however, decreased the viability by 50% in only 50 min, and by about 80% in 170 min (Figure 2e). The efficacy of the antibacterial activity of Kana-loaded MSN–AuNC@Lys was further investigated at various particle concentrations ($20, 80, 120, \text{ and } 200 \text{ }\mu\text{g mL}^{-1}$) for up to 3 h (Figure 3a).^[33] Kana-loaded MSN–AuNC@Lys were able to inhibit the growth of *E. coli* by more than 96% at a concentration of $200 \text{ }\mu\text{g mL}^{-1}$ over a short period of time. A concentration of $20 \text{ }\mu\text{g mL}^{-1}$ resulted in inhibiting 73% of bacteria over the same period of time. Photographs of Petri dishes containing *E. coli* bacteria grown on LB agar also showed that Kana-loaded MSN–AuNC@Lys were more efficient to inhibit bacterial growth than cargo-free NPs and the *E. coli* control (Figure 3b–d). The nanofiller antibacterial activity toward *B. safensis* was also very effective (Figure S5, Supporting Information). Note that, this design showed a faster response against bacteria and better antibacterial properties when compared to other reported systems employing lysozyme.^[33]

2.5. Detection of *E. Coli* Bacteria

The loss of AuNC@Lys fluorescence was correlated qualitatively to *E. coli* concentration. *E. coli* 4×10^3 to $4 \times 10^7 \text{ CFU mL}^{-1}$ were mixed with $300 \text{ }\mu\text{g mL}^{-1}$ of Kana-loaded MSN–AuNC@Lys and incubated for 3 h. The fluorescence intensity was detected at λ_{max} 580 nm. The fluorescence intensity of AuNC@Lys

decreased linearly with the increase in *E. coli* concentration over this range. The calibration function for the *E. coli* analysis is $I = 0.12848c + 64.7947$ (with a good linearity $r^2 = 0.948$) where I is the fluorescence intensity and c is the concentration of *E. coli* (Figure S6, Supporting Information).

2.6. Fabrication and Characterization of the Mixed Matrix Coating

The antibacterial MSN–AuNC@Lys nanofillers were then mixed with the PEO–PBT copolymer (also known as polyactive) which is a promising flexible, environmentally friendly, biocompatible, and cost-effective polymer for manufacturing membranes.^[49–52] Polyactive is amphiphilic and soluble in tetrahydrofuran (THF) which allows a homogenous mixture with an aqueous dispersion of MSN–AuNC@Lys to avoid phase separation or precipitation during the membrane preparation. Mixed membranes of 50 μm in thickness were fabricated employing a THF/H₂O mixture (80:20, v:v) of polyactive with or without 10 wt% of MSN–AuNC@Lys NPs via a slow evaporation process of the solvent at room temperature (Figure 4a,b). The presence of the MSN–AuNC@Lys nanofiller was confirmed by comparing scanning electron microscope (SEM) images of the pure and mixed membrane coatings (Figure 4c,d). Atomic force microscopy (AFM) images correlated these results with a significant increase of the surface roughness from 17 nm in the polyactive membrane coating to 116 nm in the polyactive-nanofiller coating (Figure 4e,f). In order to visualize the particles, SEM and TEM of a cross-section of the mixed membrane were then performed and showed the incorporation of

the nanofillers (Figure 4g–i). High magnification TEM micrographs also revealed that the hexagonal porosity of MSN was intact (Figure 4i). Thermogravimetric analysis (TGA) of the nanofillers, the nanofiller-free membrane, and the membrane-nanofillers verified the incorporation of about 10 wt% of nanofillers (Figure S7, Supporting Information). The thermal decomposition of the polymer matrix started at 400 °C while the nanofillers decomposed in two steps: a minor fraction from 250 to 500 °C and the major fraction at around 550 °C. This analysis also demonstrated that the presence of the nanofillers did not decrease the thermal stability of the polyactive polymer.

2.7. Drug Release and Biocompatibility of the Mixed Membrane

The *E. coli* bacteria-responsiveness of the mixed membrane was tested first. The release of Kana drugs was obtained in the presence of bacteria while the drugs remained loaded in LB broth (Figure 5a,b). As observed with the cargo-loaded MSN–AuNC@Lys nanofillers, the release of the Kana cargos from the mixed membrane was also delayed for approximately 50 min ($\lambda_{\text{abs}} = 255 \text{ nm}$, Figure 5b). The biocompatibility of the mixed membrane coating was then evaluated by the trypan blue dye exclusion assay.^[53] The number of viable cells was counted using a hemocytometer and the percentage of viable cells was correlated to the number of cells in the control. A section of the membrane with a diameter of 10 mm was soaked in methanol for 5 min, washed, and then placed into a 24-well plate. A solution of HCT-116 cells was added to each well containing the membrane for 2 d and membrane-free wells served as positive controls. Two days after cell culturing on the membrane, their

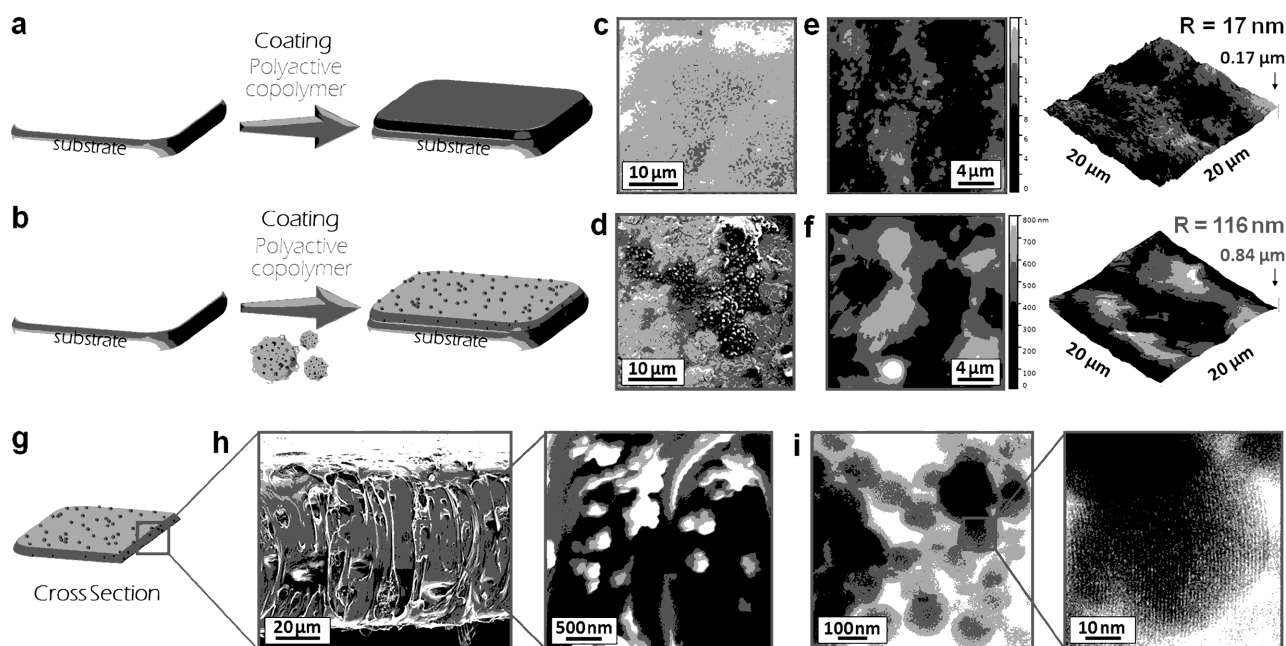


Figure 4. Representation of the polymer coating a) without and b) with the antibacterial nanofillers and c,d) the corresponding SEM and e,f) AFM micrographs. The roughness (R) observed on the membrane by AFM varied and supported the particle doping of the polyactive membrane. g) Representation of a cross-section of the membrane on which h) SEM and i) TEM analyses were performed to verify the uniform dispersion of the mesoporous particles into the membrane.

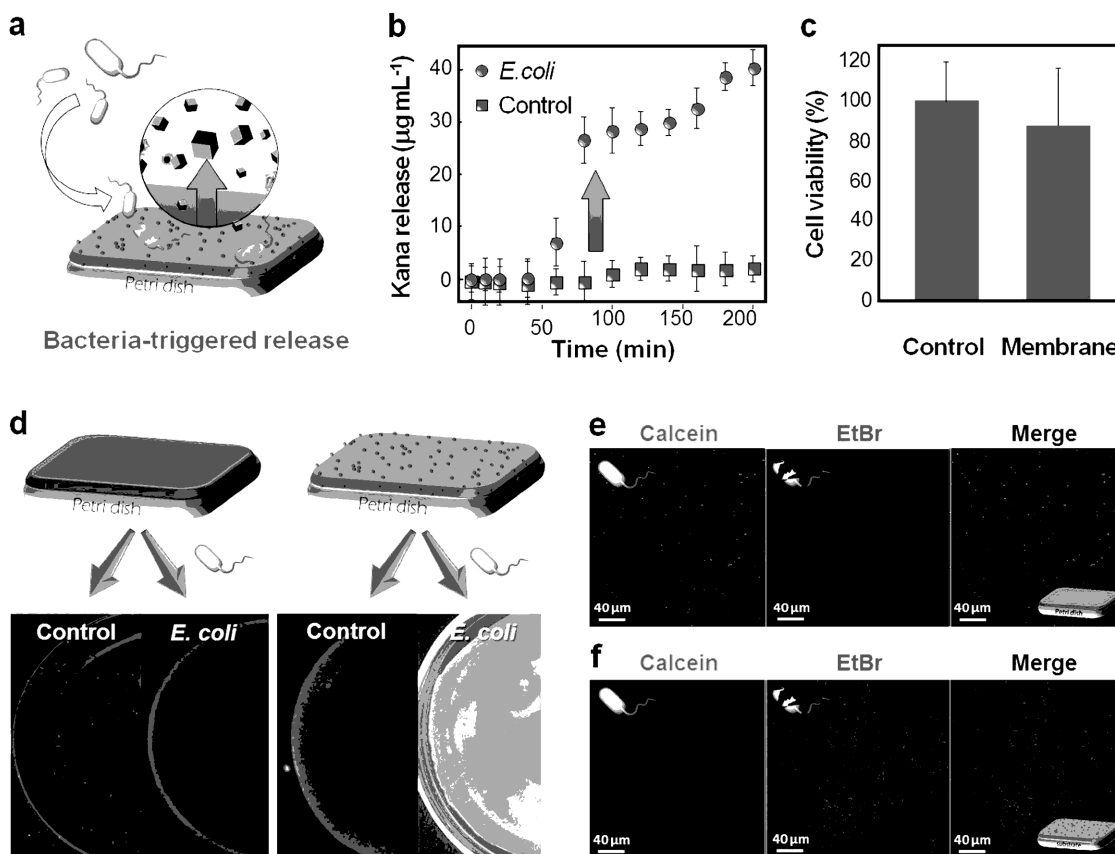


Figure 5. a) Representation the bacteria-responsiveness of the smart membrane for the release of Kana drugs (represented by cubes). b) Kana release profiles from the mixed membrane in the presence of *E. coli* bacteria or in LB broth. c) Cell viability assay of the membrane showing the non-significant cytotoxicity of the device coating. d) The nanofiller-free and nanofiller-doped membranes was immersed (or not) with *E. coli* containing broth. The AuNC fluorescence was quenched upon the *E. coli* exposure. CLSM images of *E. coli* stained with a fluorescent cell viability marker (live–dead assay) for e) the nanofiller-free and f) nanofiller-doped membranes. Viable bacteria appeared as green dots and non-viable as red dots.

viability rate was determined. The viability of the cultured cells was 86% which is remarkably low despite the high content of the membrane in this test (Figure 5c).

2.8. Antibacterial Activity of the Mixed Membrane

E. coli bacteria were then poured on the membrane and left for 8 h (3 mL, OD₆₀₀: 0.6 = 4.8×10^8). As shown in Figure 5d which compares the membrane with or without nanofillers, the fluorescence of AuNC@Lys was sharply quenched in the presence of *E. coli* which indicated the lysozyme activity and the kanamycin release. In order to confirm the antimicrobial properties associated with the release of the drug, live–dead assay were performed. In this assay, the viable and dead bacteria were respectively stained in green by calcein and in red by ethidium bromide (Figure 5e,f). Using only polyactive membranes, most of the bacteria remained viable as shown with green calcein color (Figure 5e). Conversely, employing the MSN–AuNC@Lys mixed membrane coating, the image was covered with red dots indicating high bacterial death (Figure 5f). In the absence of the bacteria the nanofillers remained in the coating after 10 d in various fluids (H₂O pH 5 and 7, saline) as shown by inductively coupled plasma-mass spectrometry (ICP-MS) analysis

(see Table S1 in the Supporting Information). Differential scanning calorimetry (DSC) was also carried out as a quality control verification of the thermal stability of the composite membranes before and after exposure to bacteria (Figure S8, Supporting Information). The DSC data showed minor shifts in the crystallization temperature peaks with the presence of nanofillers and no other peaks were detected, which implied that there was no phase transition in the composite membrane even after exposure to bacteria which supported the proper stability of the membrane for the targeted application.

2.9. Coating X-Ray Dental Imaging Plates

The mixed membrane was then applied as a protective smart coating of X-ray dental image plates. A photostimulable phosphor (PSP) plate was coated with the developed smart membrane. Such imaging plates are usually inserted into a plastic sleeve or a “barrier envelope” prior to insertion into the mouth of the patient to acquire X-ray dental images. A major limitation of the PSP plates, however, is the possibility of transferring contaminated material to patients when the protective envelope of the plate is damaged. Coating the PSP plate with MSN–AuNC@Lys mixed membrane coating showed a bright

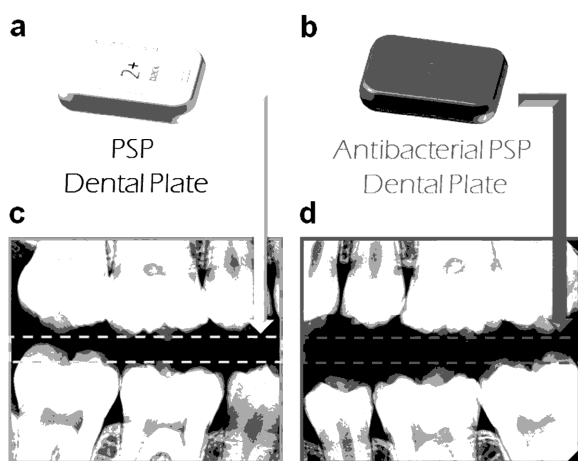


Figure 6. Representation of a PSP dental plate a) without or b) with the smart bacteria-responsive coating. X-ray radiographic dental images using the c) uncoated and d) the coated PSP plate. Both coated and uncoated plates provided high-resolution images.

red color in the absence of bacterial contamination (Figure 6a, see photograph in Scheme 1d). At low bacterial contamination (4×10^3 CFU mL⁻¹), the antibacterial nanofillers could quickly inhibit the bacterial infection and a decrease in red fluorescence was observed (Figure 6b, see photograph in Scheme 1e). However, only a blue color was obtained in the case of high bacterial contamination (4×10^7 CFU mL⁻¹) as shown in Figure 6c. Most importantly, the designed smart coating did not jeopardize the quality of the dental images obtained with the PSP (see Figure 6c,d). The bacteria-responsive MSN–AuNC@Lys-polyactive coating thus provides a safer practical application of PSP medical devices with a straightforward optical detection test to assess their antimicrobial effectiveness.

3. Conclusions

A smart dual-functional membrane with sensing and antibacterial properties was developed for the coating of X-ray dental imaging devices. These two properties were garnered into the polymer coating material via the incorporation of drug-loaded mesoporous silica nanoparticles capped with gold nanoclusters@lysozyme colloids which have an intense red fluorescence in the absence of bacteria. In the presence of *E. coli* bacteria, however, the red fluorescence was quenched as the clusters were detached from the silica particles while releasing the antimicrobial drugs. The absence of fluorescence on the surface of the plate led to a blue color under UV light and indicated the bacterial contamination; conversely, a red fluorescent surface signaled a bacteria-free environment. The MSN–AuNC@Lys-polyactive smart coating was characterized with multiple techniques including electron microscopies and spectroscopic methods, and the sensing and bacteria-triggered drug release features were demonstrated in vitro. The practical utility of this coating was then showcased on X-ray dental imaging plates which are prone to oral bacteria contamination. The system showed reproducible detection and inhibition of the bacterial growth with high-quality X-ray dental images which proved its

promising real-life applicability. Moreover, this coating strategy could be further expanded to include the monitoring and inhibition of bacterial contamination on hospital surfaces, medical equipment, and other radiographic patient care devices.

4. Experimental Section

Materials: Milli-Q water (18.2 mΩ; Millipore Co., USA) was used in all experiments and to prepare all buffers. Cetyltrimethylammonium bromide (CTAB), tetraethylorthosilicate (TEOS), sodium hydroxide (NaOH), (3-aminopropyl)triethoxysilane (APTES), methanol (MeOH), ethanol (EtOH), lysozyme from chicken egg white (Lys), PBS, THF, chloroauric acid (HAuCl₄·4H₂O), RhB, kanamycin (Kana) sulfate and trypsin were purchased from Sigma-Aldrich. Calcein, ethidium bromide, and MTT were purchased from Life Technologies. Bacto agar and LB broth were purchased from Becton and Dickinson (BD). MCF-7 and HCT-116 cell lines were purchased from ATCC. (PEO–PBT) copolymer was received from IsoTis Orthobiologics. All the chemicals were used as received without further purification.

Preparation of Cargo-Loaded MSN–AuNC@Lys—Preparation of MSN^[37]: First, CTAB (0.80 g) was stirred in deionized water (384 mL). Then, a concentrated aqueous solution of NaOH (2.8 mL, 2 M) was added, and the temperature of the solution was set to 80 °C. After 30 min, TEOS (4 mL) was added dropwise while stirring and the sol–gel process was conducted for 2 h. Finally, the MSN–CTAB suspension was cooled down to room temperature, centrifuged at 14 000 rpm for 15 min, washed with deionized water and methanol, and dried under vacuum for few hours.

Preparation of Cargo-Loaded MSN–AuNC@Lys—Preparation of MSN–NH₂^[41,45]: Non-extracted MSN–CTAB (200 mg) were suspended in anhydrous toluene (30 mL), APTES (100 μL) was added to the mixture, and the solution was refluxed for 24 h. Then, the solution was cooled down to room temperature, centrifuged at 14 000 rpm for 10 min, washed several times with EtOH, and dried at room temperature overnight. The resulting amino functionalized NPs were refluxed for 16 h in a mixture of methanol (80 mL) and concentrated HCl (1 mL, 37%), filtered, and washed extensively with water and ethanol. Two other extractions were carried out via ammonium nitrated ethanol solutions (6 g L⁻¹), followed by ethanol washings to ensure the complete CTAB removal. The resulting surfactant-free MSN–NH₂ were dried under vacuum for few hours.

Preparation of Cargo-Loaded MSN–AuNC@Lys—Preparation of AuNC@Lys: AuNC@Lys were synthesized according to a previously reported procedure.^[34] Briefly, an aqueous solution of HAuCl₄ solution (5 mL, 10×10^{-3} M) was added to a lysozyme solution (5 mL, 50 mg mL⁻¹) under vigorous stirring at 37 °C. After 10 min, an aqueous solution of NaOH (500 mL, 1 M) was introduced, and the mixture was incubated at 37 °C for 12 h. The final solution was stored at 4 °C.

Preparation of Cargo-Loaded MSN–AuNC@Lys—Preparation of MSN–AuNC@Lys: MSN–NH₂ (20 mg) were dispersed in PBS (20 mL, 10×10^{-3} M, pH 7.4), and the solution was sonicated for 1 min. The as-prepared AuNC@Lys solution (5 mL) was then added into the MSN–NH₂ solution and the mixture was stirred at room temperature for 12 h. Finally, the resulting MSN–AuNC@Lys product was collected by centrifugation (4000 rpm, 10 min) and washed with PBS (10×10^{-3} M) several times.

Preparation of Cargo-Loaded MSN–AuNC@Lys—Preparation of Cargo-Loaded MSN–AuNC@Lys: MSN–NH₂ (100 mg) were dispersed in PBS (25 mL, 10×10^{-3} M, pH 7.4), mixed with RhB or Kana cargos (200 mg), and stirred at room temperature for 24 h. The RhB-loaded or Kana-loaded MSN–NH₂ were then collected via centrifugation (4000 rpm, 10 min), washed once with deionized water, and dried under vacuum for few hours. The AuNC@Lys PBS solution was mixed with cargo-loaded MSN–NH₂ and stirred for 6 h, followed by centrifugation and repeated washings with PBS. The amount of loaded Kana was determined by the Beer–Lambert law: $A = \epsilon \cdot c \cdot l$, where A is the absorbance, c is the Kana concentration, l is the path length of the sample cell (1 cm), and ϵ is the molar extinction coefficient of Kana ($143.40 \text{ m}^{-1} \text{ cm}^{-1}$, at 255 nm and pH 7).

Bacterial Studies—Bacterial Viability Determination: *E. coli* or *B. safensis* were cultured in LB medium at 37 °C on a shaker bed at 200 rpm for 4–6 h. Then the concentration of bacteria, corresponding to an optical density of 0.2 at 600 nm for 1.6×10^8 CFU mL⁻¹ diluted with LB medium, was measured by using UV-vis spectroscopy (Novaspec Plus Visible Spectrophotometer). Bacterial suspension (20 µL of 1.6×10^8 CFU mL⁻¹) was added into LB medium for each well. Then, different concentrations of NPs (20, 80, 120, and 200 µg mL⁻¹) were separately added into 24-well plates and shaken at 37 °C on a shaker bed at 200 rpm for 3 h.^[33] A NPs-free solution was used as a positive control. The bacterial viability was determined by OD_{600nm}. Each concentration was prepared and measured in triplicate, and all experiments were repeated at least twice in parallel. Then, solutions of the control (10 µL), of RhB-loaded MSN–AuNC@Lys (10 µL, 20 µg mL⁻¹), and of Kana-loaded MSN–AuNC@Lys (10 µL, 20 µg mL⁻¹) were plated on LB agar and incubated at 37 °C overnight to count the number of bacterial colonies.

Bacterial Studies—Dual Activity of AuNC@Lys and Kana: Kana release was monitored by UV-vis at 255 nm.^[54] Kana–MSN–AuNCs@Lys (200 µg mL⁻¹) were incubated with *E. coli* (1.6×10^8 CFU mL⁻¹) at 37 °C under gentle shaking. The amount of kanamycin released was calculated by Beer–Lambert law. The loss of AuNCs fluorescence was detected by fluorescence spectrophotometer at 580 nm.

Polymer Coating—Pristine Polymer Coating: The PEO–PBT polyactive copolymer (3 wt%) was dissolved in THF (4 mL) and refluxed overnight. The resulting polymer solution was transferred into a glass Petri dish and then dried under air for 24 h at room temperature to ensure a slow evaporation process. Finally, the composited membrane was placed in a vacuum oven to evaporate potential water residues.

Polymer Coating—Composite Coating: Kana-loaded MSN–AuNC@Lys were dispersed in deionized water at a concentration of 20 mg mL⁻¹. A fraction of this solution (1 mL) was then diluted in THF (4 mL) and the resulting mixture was sonicated for 1 h. Then, the PEO–PBT polyactive copolymer (3 wt%, 150 mg) was added and the solution was refluxed overnight. The same evaporation procedure used for the pristine film was followed to obtain the composite coating.

Polymer Coating—Coating of the Dental Device: The previous composite solution was spin coated on PSP plates with a controlled thickness. The coated dental plate was dried under air for 24 h at room temperature to ensure a slow evaporation process. Finally, the composited membrane was placed in a vacuum oven to evaporate potential water residues.

Live–Dead Assay: The Kana-loaded MSN–AuNC@Lys–Polyactive membrane was completely immersed into a bacterial suspension (5 mL) in a sterile 15 mL conical tube. The membrane was incubated at room temperature for 8 h. The live–dead assay was performed by immersing the membrane in the live–dead assay reagent, which was prepared according to the manufacturer. Then, two washings were performed with PBS. The membrane was mounted on a slide and imaged by laser scanning confocal microscopy.

Cell Culture: MCF-7 and HCT-116 cells were seeded at a density of 5×10^3 cells per well. Cells were cultured in an Eagle's Minimal Essential Medium (EMEM) containing 10% of Fetal Bovine Serum (FBS) and 0.1% of penicillin–streptomycin at 37 °C in a humidified 5% CO₂ atmosphere. The media of MCF-7 was supplemented with 0.01 mg mL⁻¹ insulin.

MTT Assay: The cell viability was tested by the MTT (3-(4,5-dimethylthiazol-2-yl)-2,5 diphenyltetrazolium bromide, Life Technologies, Carlsbad, CA, USA) assay following the instructions of the manufacturer. Briefly, MCF-7 and HCT-116 cells (5×10^3 cells per well) were seeded onto a 96-well plate. On the following day, the culture medium was changed, and cells were incubated with different concentrations (200, 100, 50, 25, 12.5, and 6.25 µg mL⁻¹) of Kana-loaded MSN–AuNC@Lys in 200 µL of fresh medium at 37 °C for 24 h. After 24 h, the medium was discarded, and a prepared culture medium containing 12×10^{-3} M MTT solution was added to each well, including a negative control of culture media alone. After 3 h incubation, the medium was removed from the wells. Then 50 µL of DMSO was added to each well and mixed thoroughly for 10 min. The absorbance was measured at 540 nm using a microplate spectrophotometer (xMark Microplate Absorbance Spectrophotometer).

Trypan Blue Dye Exclusion Assay: The membrane was cut into 1 cm pieces. Each piece was placed in a well of the 24-well plate. Membrane-free wells were used as positive controls. HCT-116 cells were seeded at a density of 5×10^3 cells per well in an EMEM medium at 37 °C in a humidified 5% CO₂ atmosphere for 2 d. The media was changed every 12 h. At the end of the culture period, the medium was removed from the culture dish, cells were collected by adding trypsin and centrifugation (1000 rpm, 5 min). Cells were washed with PBS twice and trypan blue staining of the cells was performed by adding 50 mL trypan blue (4%) to 50 mL cell suspension. A hemocytometer was filled and the cells were observed under an inverted microscope for total and viable cell counting. Viable cells were gray and dead cells were blue.

ICP-MS Particle Leaching Experiments: The experiments were performed on the mixed matrix coating in three media: in deionized water at pH 7, in deionized water at pH 5, and in a saline solution. The authors studied the leaching of Au from the coating for 10 d. The resulting solutions were analyzed every 24 h for 10 d with an inductively coupled plasma mass spectrometry (Elan DRC II, PerkinElmer) to quantify the concentration of gold. The membranes were then digested and the results were presented in terms of percentage of Au released compared to the total amount of Au in the membrane. The results revealed the absence of Au release in the three media, as the Au quantification yielded percentages below the accuracy limits of the instrument.

Apparatus and Methods: The surface morphologies of the pure and composite membrane were investigated by field emission scanning electron microscopy using SEM Quanta 600. Standard TEM images were collected using a Tecnai G2 Spirit TWIN 20–120 kV/LaB6. The NPs were dispersed in ethanol and drop cast on a lacy copper grid and dried for 1 h prior to analysis. The chemical composition of the NPs was measured by FTIR spectrometer in the range of 500–4000 cm⁻¹. The decomposition behavior of the composites was studied using a TGA (TG 209 F1 Iris, Netzsch, Germany) under nitrogen from 30 to 1000 °C at a ramping rate of 10° min⁻¹. XPS data were collected by an Axis Ultra instrument (Kratos Analytical) under ultrahigh vacuum (<10⁻⁸ Torr) and by using a monochromatic Al K α X-ray source operating at 150 W. AFM images were acquired using an Agilent 5400 SPM instrument (USA). Porosimetry analyses were performed using a “Micromeritics” (ASAP 2420) instrument at 77 K. ICP-MS data was obtained using a Perkin Elmer Elan DRC-II instrument.

Supporting Information

Supporting Information is available from the Wiley Online Library or from the author.

Acknowledgments

S.K.A. and M.A.H. contributed equally to this work. The authors gratefully acknowledge Dr. Abdallah Abdallah from King Abdullah University of Science and Technology (KAUST) for providing *E. coli*. The authors also thank Dr. Asma'a A. Al-Ekrish from King Saud University and Dr. Alhasan Alsaiani from King Abdulaziz University College of Dentistry for providing and testing the dental imaging plates. The authors declare no competing financial interest.

Received: October 5, 2016

Revised: December 8, 2016

Published online:

[1] P. Maurette, C. A. M. R. Sfa, *Ann. Fr. Anesth. Reanim.* **2002**, 21, 453.

[2] V. Sambhy, M. M. MacBride, B. R. Peterson, A. Sen, *J. Am. Chem. Soc.* **2006**, 128, 9798.

- [3] K. C. L. Black, T. S. Sileika, J. Yi, R. Zhang, J. G. Rivera, P. B. Messersmith, *Small* **2014**, *10*, 169.
- [4] R. O. Darouiche, *Clin. Infect. Dis.* **1999**, *29*, 1371.
- [5] S. Taheri, A. Cavallaro, S. N. Christo, L. E. Smith, P. Majewski, M. Barton, J. D. Hayball, K. Vasilev, *Biomaterials* **2014**, *35*, 4601.
- [6] C. Aymonier, U. Schlotterbeck, L. Antonietti, P. Zacharias, R. Thomann, J. C. Tiller, S. Mecking, *Chem. Commun.* **2002**, 3018.
- [7] S. H. Park, Y. S. Ko, S. J. Park, J. S. Lee, J. Cho, K. Y. Baek, I. T. Kim, K. Woo, J. H. Lee, *J. Membr. Sci.* **2016**, *499*, 80.
- [8] L. C. Huang, S. Zhao, Z. Wang, J. H. Wu, J. X. Wang, S. C. Wang, *J. Membr. Sci.* **2016**, *499*, 269.
- [9] H. J. Jeon, S. C. Yi, S. G. Oh, *Biomaterials* **2003**, *24*, 4921.
- [10] X. Z. Li, H. Nikaido, K. E. Williams, *J. Bacteriol.* **1997**, *179*, 6127.
- [11] P. J. Finley, A. Peterson, R. E. Huckfeldt, *Wounds* **2013**, *25*, 84.
- [12] C. Gunawan, W. Y. Teoh, C. P. Marquis, R. Amal, *Small* **2013**, *9*, 3554.
- [13] F. Pulizzi, *Nat. Nano* **2016**, *18*, DOI: 10.1038/nnano.2016.11.
- [14] V. B. Schwartz, F. Thetiot, S. Ritz, S. Putz, L. Choritz, A. Lappas, R. Forch, K. Landfester, U. Jonas, *Adv. Funct. Mater.* **2012**, *22*, 2376.
- [15] M. J. Wang, J. L. Coffey, K. Dorraj, P. S. Hartman, A. Loni, L. T. Canham, *Mol. Pharmaceut.* **2010**, *7*, 2232.
- [16] H. X. Wu, L. Tan, Z. W. Tang, M. Y. Yang, J. Y. Xiao, C. J. Liu, R. X. Zhuo, *ACS Appl. Mater. Inter.* **2015**, *7*, 7008.
- [17] I. Makarovskiy, Y. Boguslavskiy, M. Alesker, J. Lellouche, E. Banin, J. P. Lellouche, *Adv. Funct. Mater.* **2011**, *21*, 4295.
- [18] F. Kayaci, Y. Ertas, T. Uyar, *J. Agric. Food Chem.* **2013**, *61*, 8156.
- [19] S. Woranuch, R. Yoksan, *Carbohydr. Polym.* **2013**, *96*, 586.
- [20] M. L. Noble, P. D. Mourad, B. D. Ratner, *Biomater. Sci.* **2014**, *2*, 893.
- [21] S. Y. Wong, Q. Li, J. Veselinovic, B. S. Kim, A. M. Klibanov, P. T. Hammond, *Biomaterials* **2010**, *31*, 4079.
- [22] C. M. Xie, X. Lu, K. F. Wang, F. Z. Meng, O. Jiang, H. P. Zhang, W. Zhi, L. M. Fang, *ACS Appl. Mater. Interfaces* **2014**, *6*, 8580.
- [23] M. S. Ganewatta, K. P. Miller, S. P. Singleton, P. Mehrpouya-Bahrami, Y. P. Chen, Y. Yan, M. Nagarkatti, P. Nagarkatti, A. W. Decho, C. Tang, *Biomacromolecules* **2015**, *16*, 3336.
- [24] P. K. S. B. Mural, A. M. S. Rana, A. Shukla, B. Padmanabhan, S. Bhadra, G. Madras, S. Bose, *J. Mater. Chem. A* **2014**, *2*, 17635.
- [25] Y. Tal-Gan, D. M. Stacy, M. K. Foegen, D. W. Koenig, H. E. Blackwell, *J. Am. Chem. Soc.* **2013**, *135*, 7869.
- [26] M. van Oosten, T. Schafer, J. A. C. Gazendam, K. Ohlsen, E. Tsompanidou, M. C. de Goffau, H. J. M. Harmsen, L. M. A. Crane, E. Lim, K. P. Francis, L. Cheung, M. Olive, V. Ntziachristos, J. M. van Dijk, G. M. van Dam, *Nat. Commun.* **2013**, *4*, 2584.
- [27] S. A. Burt, V. T. Ojo-Fakunle, J. Woertman, E. J. Veldhuizen, *PLoS One* **2014**, *9*, e93414.
- [28] K. Glinel, P. Thebault, V. Humblot, C.-M. Pradier, T. Jouenne, *Acta Biomater.* **2012**, *8*, 1670.
- [29] X. N. Li, H. Kong, R. Mout, K. Saha, D. F. Moyano, S. M. Robinson, S. Rana, X. R. Zhang, M. A. Riley, V. M. Rotello, *ACS Nano* **2014**, *8*, 12014.
- [30] J. Zhou, A. L. Loftus, G. Mulley, A. T. A. Jenkins, *J. Am. Chem. Soc.* **2010**, *132*, 6566.
- [31] P. H. Chan, S. Y. Wong, S. H. Lin, Y. C. Chen, *Rapid Commun. Mass Spectrom.* **2013**, *27*, 2143.
- [32] M. Kiristi, V. V. Singh, B. E. F. de Avila, M. Uygun, F. Soto, D. A. Uygun, J. Wang, *ACS Nano* **2015**, *9*, 9252.
- [33] L. L. Li, H. Wang, *Adv. Healthcare Mater.* **2013**, *2*, 1351.
- [34] H. Wei, Z. D. Wang, L. M. Yang, S. L. Tian, C. J. Hou, Y. Lu, *Analyst* **2010**, *135*, 1406.
- [35] K. Pyo, V. D. Thanthirige, K. Kwak, P. Pandurangan, G. Ramakrishna, D. Lee, *J. Am. Chem. Soc.* **2015**, *137*, 8244.
- [36] H. C. Chang, Y. F. Chang, N. C. Fan, J. A. Ho, *ACS Appl. Mater. Interfaces* **2014**, *6*, 18824.
- [37] J. G. Croissant, C. Qi, M. Maynadier, X. Cattoën, M. Wong Chi Man, L. Raehm, O. Mongin, M. Blanchard-Desce, M. Garcia, M. Gary-Bobo, J.-O. Durand, *Front. Mol. Biosci.* **2016**, *3*, DOI: 10.3389/fmolb.2016.00001.
- [38] H. A. Meng, M. Liong, T. A. Xia, Z. X. Li, Z. X. Ji, J. I. Zink, A. E. Nel, *ACS Nano* **2010**, *4*, 4539.
- [39] J. G. Croissant, X. Cattoën, M. Wong Chi Man, J.-O. Durand, N. M. Khashab, *Nanoscale* **2015**, *7*, 20318.
- [40] J. G. Croissant, O. Mongin, V. Hugues, M. Blanchard-Desce, X. Cattoën, M. Wong Chi Man, V. Stojanovic, C. Charnay, M. Maynadier, M. Gary-Bobo, M. Garcia, L. Raehm, J.-O. Durand, *J. Mater. Chem. B* **2015**, *3*, 5182.
- [41] S. Dib, M. Boufatit, S. Chelouaou, F. Sadi-Hassaine, J. Croissant, J. Long, L. Raehm, C. Charnay, J. O. Durand, *RSC Adv.* **2014**, *4*, 24838.
- [42] H. M. Z. Song, J. I. Zink, N. M. Khashab, *Part. Part. Syst. Charact.* **2015**, *32*, 307.
- [43] J. Croissant, J. I. Zink, *J. Am. Chem. Soc.* **2012**, *134*, 7628.
- [44] B. Rühle, P. Saint-Cricq, J. I. Zink, *ChemPhysChem* **2016**, *17*, 1769.
- [45] J. G. Croissant, D. Zhang, S. Alsaiari, J. Lu, L. Deng, F. Tamanoi, A. M. AlMalik, J. I. Zink, N. M. Khashab, *J. Controlled Release* **2016**, *229*, 183.
- [46] M. Ma, H. Chen, Y. Chen, X. Wang, F. Chen, X. Cui, J. Shi, *Biomaterials* **2012**, *33*, 989.
- [47] J. G. Croissant, D. Zhang, S. Alsaiari, J. Lu, L. Deng, F. Tamanoi, A. M. AlMalik, J. I. Zink, N. M. Khashab, *J. Controlled. Release* **2016**, *229*, 183.
- [48] W. Song, R.-P. Liang, Y. Wang, L. Zhang, J.-D. Qiu, *Chem. Commun.* **2015**, *51*, 10006.
- [49] G. J. Meijer, M. S. Cune, M. VanDooren, C. DePutter, C. A. VanBlitterswijk, *J. Oral Rehabil.* **1997**, *24*, 85.
- [50] G. J. Beumer, C. A. Vanblitterswijk, M. Ponc, *J. Biomed. Mater. Res.* **1994**, *28*, 545.
- [51] A. M. Radder, H. Leenders, C. A. Vanblitterswijk, *J. Biomed. Mater. Res.* **1994**, *28*, 141.
- [52] C. Du, P. Klasens, R. E. Haan, J. Bezemer, F. Z. Cui, K. de Groot, P. Layrolle, *J. Biomed. Mater. Res.* **2002**, *59*, 535.
- [53] R. I. Freshney, *Culture of Animal Cells: A Manual of Basic Technique and Specialized Applications*, Wiley, New York **1987**.
- [54] C. Khurana, A. K. Vala, N. Andhariya, O. P. Pandey, B. Chudasama, *Environ. Sci.: Processes Impacts* **2014**, *16*, 2191.